We are IntechOpen, the world's leading publisher of Open Access books Built by scientists, for scientists

4,800
Open access books available

122,000
International authors and editors

135M
Downloads

Our authors are among the

154
Countries delivered to

TOP 1%
most cited scientists

12.2%
Contributors from top 500 universities

WEB OF SCIENCE™

Selection of our books indexed in the Book Citation Index in Web of Science™ Core Collection (BKCI)

Interested in publishing with us?
Contact book.department@intechopen.com

Numbers displayed above are based on latest data collected.
For more information visit www.intechopen.com

2

Airborne Electromagnetic Bathymetry

Julian Vrbancich
Defence Science and Technology Organisation (DSTO)
Australia

1. Introduction

Traditional methods for measuring the water depth rely on sonar soundings. However airborne techniques offer the advantages of increased survey speed and operation over dangerous waters that may be affected by very strong tides and the presence of shoals and reefs that limit the operation of surface vessels. The airborne lidar method has been used very successfully for mapping coastal waters and relies on the difference in the time between a laser pulse (infra red wavelength) reflected from the sea surface and a separate laser pulse (blue-green wavelength) reflected from the sea floor. The depth of investigation, typically 50 to 70 m in ideal conditions, depends strongly on water clarity (turbidity), as well as other factors (e.g. sea state, surf zone, sea bottom reflection) and weather conditions. These lidar systems provide dense depth soundings, typically a grid with a laser spot spacing of 4 to 5 m, and they meet the accuracy standards of the International Hydrographic Organisation (IHO).

The airborne electromagnetic (AEM) bathymetry method is based on the AEM technique (Spies et al., 1998; Palacky & West, 1991) developed for geological exploration of electrically conducting targets, initially applied to mineral exploration. Since then, the AEM technique has also been applied to environmental studies, e.g. mapping hydrogeological features in alluvial aquifers (Dickinson et al., 2010); and salinity distribution (Fitterman and Deszcz-Pan, 1998; Hatch et al., 2010; Kirkegaard et al., 2011). The AEM method uses an airborne transmitter loop with a known magnetic moment (i.e. a magnetic dipole source) that generates a *primary* magnetic field to induce electrical currents in the ground. These currents establish a *secondary* magnetic field (the EM response) which is detected by the airborne receiver loop, shown schematically in Figure 1. The mathematical theory of this EM induction process is thoroughly reviewed by Ward & Hohman (1987), Wait (1982), Weaver (1994), West & Macnae (1991) and Grant & West (1965). The EM induction process causes the electromagnetic fields to *diffuse* slowly into the conductive medium. Nabighian (1979) showed that the transient time-domain electromagnetic (TEM) response (caused by a rapid turn-off of the transmitter current) "observed over a conducting half-space[1] or a layered earth can be represented by a simple current filament of the same shape as the transmitter loop moving downward and outwards (in the isotropic conductive medium) with a decreasing velocity and diminishing amplitude, resembling a system of "smoke rings"

[1] A "half-space" refers to an infinitely deep homogeneous earth (ground) with a given electrical conductivity.

blown by the transmitter loop" (Nabighian, 1979). This concept was later extended to a frequency domain EM response (Reid & Macnae, 1998) where the transmitter loop is powered by a continuous sinusoidal current at a pre-determined frequency.

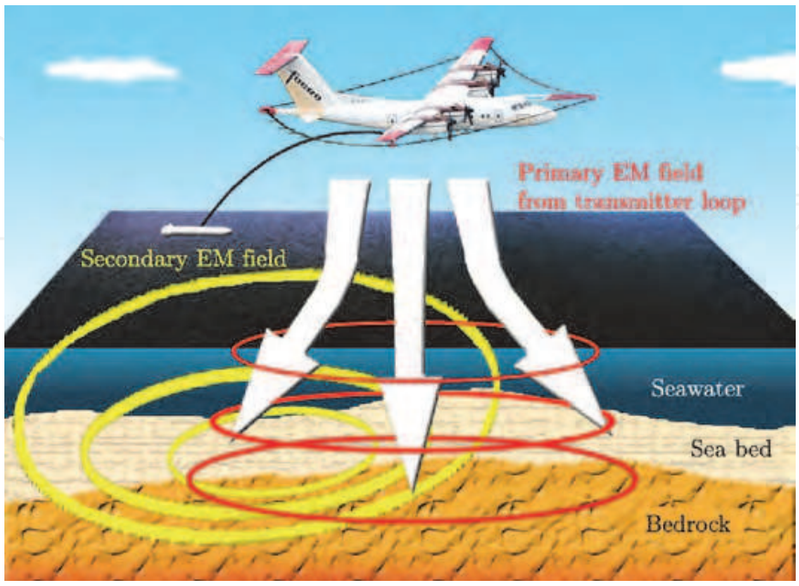

Fig. 1. Schematic diagram of the fixed-wing time-domain GEOTEM (Fugro Airborne Surveys Pty Ltd.) AEM system. The transmitter loop is mounted around the aircraft and the receiver loop is trailed behind and below the aircraft.

Thus the footprint associated with the EM induction process (to be discussed in section 3.4) is much larger than the lidar footprint. The physics of the diffusion of the EM fields in the conductive medium is such that for airborne (or ground) EM systems the horizontal resolution will always be larger than the horizontal resolution of lidar-based bathymetry systems because of the relatively small footprint of the spot laser beam. However, a distinct advantage of the AEM technique is that the EM response depends on the bulk conductivity of the medium (as well as other parameters), which in the case of seawater, is not affected by the turbidity or the presence of bubbles. Thus the interpretation of AEM data acquired over seawater is expected to provide water depths, in relatively shallow coastal waters irrespective of turbidity levels (within reasonable limits), and in the surf zone.

The simplest model for interpreting AEM data for bathymetry studies assumes a one-dimensional (1D) layered-earth structure which in its crudest form consists of two upper layers, a seawater layer overlying an unconsolidated sediment layer, with each layer defined by its electrical conductivity and thickness; these layers in turn overlie a relatively resistive[2] basement (bedrock). This two-layer model allows for a sediment layer (which may become vanishingly thin over exposed bedrock on the seafloor) and assumes no stratification in the conductivity of the seawater and sediment layers. Distinct conductive layers of seawater and/or sediment can be readily included by introducing more layers if warranted. The

[2] The electrical conductivity (S/m) is the reciprocal of electrical resistivity (Ωm) and these terms are interchanged accordingly, depending on whether one is discussing a good conductor or a poor conductor; e.g., seawater is conductive, bedrock is relatively resistive.

parameters used for inversion of the AEM data are the two thicknesses of the upper two layers, the three electrical conductivities associated with the two layers and the basement, and the elevations (and separations) of the transmitter and receiver loops above the sea surface. The thickness of the upper layer, as determined from the inversion of the AEM data, is the water depth which is the objective of the AEM bathymetry method. Where some parameters are measured directly, for example seawater conductivity and altimetry, or assumed, for example, sediment conductivity and basement resistivity, then these parameters may be held fixed or tightly constrained in the inversion process.

Given that the sediment layer and its associated conductivity are part of the layered-earth model, the thickness and conductivity of the sediment layer may also be determined in shallow waters from the AEM data. Combined with interpreted water depths (i.e. AEM bathymetry), the AEM method can therefore be used to (i) estimate the bedrock topography by combining the water depth and sediment thickness (Vrbancich, 2009; Vrbancich & Fullagar, 2007a) and (ii) map the seafloor resistivity (Won & Smits, 1986a). Combined with empirical relationships such as Archie's Equation (Archie, 1942) and assumed cementation factors for unconsolidated marine sediments (Glover, 2009), the derived seafloor resistivities can be used to estimate important seafloor properties such as density, porosity, sound speed and from these properties, acoustic reflectivity (Won & Smits, 1986a). The interpretation of AEM data to determine sediment thickness and sediment conductivity requires a well calibrated AEM system. The EM response is far more sensitive to the overlying conductive seawater layer than it is to the less conductive sediment layer and it is therefore more difficult to accurately determine the depth of the sediment-basement interface than the depth of the seawater-sediment interface. The same AEM dataset may provide bathymetric accuracy to within 1 metre and yet provide poor agreement with bedrock depths estimated from marine seismic data. The use of the AEM method for simultaneously mapping water depth and sediment thickness and conductivity is currently under investigation and for this purpose, it is important to have independent ground truth data consisting of (i) marine seismic survey data (matching the AEM survey line locations if possible) to provide an estimate of the depth to bedrock, and (ii) sediment resistivity data obtained, ideally, from bore hole sediment samples, or surficial sediment samples (extending to 3-5 m depth) obtained from vibrocore samples. A marine seismic survey and a resistivity study of vibrocore samples of shallow marine sediments has been undertaken in Jervis Bay (Vrbancich et al., 2011a) and Broken Bay (Vrbancich et al., 2011b), located approximately 150 km south and 40 km north of Sydney Harbour (~ 33.8^{o} S, 151.3^{o} E) respectively, to support the interpretation of AEM survey data to estimate depth of bedrock and sediment resistivity (Vrbancich, 2010).

1.1 Chapter outline

Section 2 discusses the initial development of AEM for bathymetric studies, and the associated application of AEM for sub-ice bathymetry and sea-ice thickness measurements. Section 3 describes helicopter and fixed-wing AEM systems, and some of the transmitter-current waveforms as well as discussing the AEM footprint that is relevant for understanding the lateral resolution. Section 4 provides some examples of the results of AEM bathymetry studies from helicopter[3] time-domain and frequency-domain surveys in

[3] Refer to Vrbancich et al., (2005a,b) and Wolfgram & Vrbancich (2007) for examples of fixed-wing AEM bathymetry studies.

Australian waters, comparing the interpreted water depths with known values. Section 5 (Conclusion) summarises the important findings and briefly discusses future directions.

2. Development of the AEM bathymetry method – initial studies

Initial studies in the use of AEM for bathymetric mapping took place in the 1980s. Morrison and Becker (1982) were the first to consider the use of AEM systems for mapping water depths in a feasibility report commissioned by the US Office of Naval Research (ONR) to support rapid airborne bathymetric mapping in shallow coastal waters. Morrison and Becker (1982) investigated both time domain and frequency domain systems existing at the time and concluded that frequency-domain systems would be limited to a depth of approximately 20 m and that the INPUT[4] fixed-wing time-domain system, with a lower operating base frequency, was suitable for measurement depths of 50 to 60 m. This feasibility study was followed by single flight line field trials in Nova Scotia and New Brunswick (Canada) using the INPUT system over waters that were predominantly less than about 20 m in depth, resolving water depths to about 40 m with approximately 2 m accuracy as determined by comparison with soundings on coastal charts (Becker et al., 1984; Becker et al., 1986; Zollinger, 1985; Zollinger et al., 1987).

During this period of study, Won and Smits (1985, 1986b, 1987a), and Son (1985), also investigated the use of helicopter frequency-domain AEM for bathymetric applications. Based on field trials conducted in the Cape Cod Bay area (Massachusetts, USA) using a DIGHEM^{III} AEM system (Fraser, 1978), Won and Smits (1985, 1986b, 1987a) showed that excellent agreement in water depths was obtained with acoustic profiles down to depths of about 13 to 20 m corresponding to one and one and a half skin depths at 385 Hz (the lowest of the 2 frequencies used in the DIGHEM^{III} survey). The same dataset was also used to derive continuous profiles of seawater and seabed conductivity (Won & Smits, 1986a, 1987b). Bergeron and co-workers (1989) examined the same Cape Cod Bay dataset using a different method to invert the AEM data, to obtain good agreement with measured altimetry, seawater conductivity and known water depths. Bryan et al. (2003) used field data obtained over marsh and estuarine waters in Barataria Basin (Louisiana, USA) with a frequency domain AEM system using a primary waveform digitally constructed from six harmonic frequencies (Mozley et al., 1991a,b). The results of their inversions showed good agreement with measured water conductivities and depths, identifying horizontal water layers with the less saline, less conductive, fresher water layer overlying a more saline, more conductive water layer. The same instrumentation was used by Mozley et al. (1991a,b) in field trials at Kings Bay (Georgia, USA) to successfully map seawater depths and conductivity, and variations in seafloor sediment conductivity, and by Pelletier and Holladay (1994) to map bathymetry, sediment and water properties in a complex coastal environment located at Cape Lookout, North Carolina, USA.

2.1 Airborne electromagnetic bathymetry and sea ice thickness measurements

The EM response is sensitive to sub-metre variations in the altitude of the transmitter and receiver loops above the conductive seawater layer. This sensitivity has implications for measuring sea ice thickness. If the AEM data is also inverted for altitude, then the thickness

[4] INduced PUlse Transient; a trademark of Barringer Research Ltd.

of any sea ice covering the seawater can be determined by subtracting the elevation above the surface of the relatively resistive sea ice (measured with laser altimetry) from the altitude above the seawater (Becker & Morrison, 1983; Kovacs & Holladay, 1990; Reid et al., 2003a; Haas et al., 2009). This method relies on the conductivity contrast between sea ice and seawater. As sea ice ages, brine is expelled decreasing its conductivity. The seawater conductivity is typically 2.5 – 2.6 S/m, approximately two orders of magnitude larger than sea ice conductivity and at the relatively low frequencies used in frequency-domain AEM systems (typically 50 Hz to 100 kHz), the primary and induced secondary magnetic fields effectively "see through" the sea ice. The AEM system can therefore be used to measure sea ice thickness and also sub-ice bathymetry (Kovacs & Valleau, 1987; Pfaffling & Reid, 2009) in shallow waters. This same EM induction technique can also be applied using ship-borne sensors (Reid et al., 2003a; Reid et al., 2003b; Haas et al., 1997). Unlike the AEM bathymetry method which usually assumes a layered earth model for 1D inversion, determining the structure of three-dimensional sea ice keels (pressure ridges below the sea surface) with thicknesses that may reach 6 to 10 m may require the use of 2D and 3D EM modelling and inversion procedures (Reid et al., 2003a; Liu & Becker, 1990; Liu et al., 1991; Soininen et al., 1998) in order to minimise underestimating the thickness of the ice keels that results from smoothing of the EM response over the AEM system footprint (Kovacs et al., 1995; Liu & Becker, 1990) and interpretation using 1D inversion models.

3. AEM systems: Time-domain and frequency-domain

AEM systems operate in the frequency domain (frequency electromagnetic, FEM) or in the time domain (transient electromagnetic, TEM)[5]. Helicopter AEM systems typically operate in either the frequency domain or time domain, whilst fixed-wing AEM systems typically operate in the time domain. Fountain (1998) has reviewed the first 50 years of development of AEM systems from a historical perspective. A receiver loop is used to detect the secondary magnetic field induced in the ground. The recorded response is a voltage proportional to the time derivative of a component of the secondary field, typically the vertical component (dB_z/dt). In the following text, the term "bird" refers to the AEM system towed as a sling load beneath the helicopter in FEM and TEM systems, or to the receiver unit towed beneath a fixed-wing TEM system. All three types of AEM systems have been used for bathymetric investigations in Australian coastal waters.

3.1 Frequency domain helicopter AEM

The FEM system consists of several transmitter-receiver coil pairs held in a fixed rigid geometry. The transmitter-receiver coil pair separation is about 8 m or less, and the coils may be (i) placed horizontally (horizontal co-planar (HCP) configuration, vertical magnetic moment associated with the transmitter coil), (ii) or the coil pair may be rotated by 90°, so that the coils lie in the vertical plane (vertical co-planar (VCP) configuration, horizontal magnetic moment, orthogonal to the flight direction, associated with the transmitter coil), (iii) or the coil

[5] The AEM systems GEOTEM, DIGHEM, RESOLVE, HELITEM, and HeliGEOTEM (discussed in the following sections) are trademarks of Fugro Airborne Surveys Pty Ltd. QUESTEM was operated by World Geoscience Corporation since 1990 and became obsolete in 2000 after the amalgamation of World Geoscience Corporation and Geoterrex-DIGHEM Pty Ltd into the newly formed company Fugro Airborne Surveys Pty Ltd.

axes lie on the same horizontal line (vertical co-axial (VCX) configuration, horizontal magnetic moment in-line with flight direction, associated with the transmitter coil). Thus with respect to the flight direction, the HCP, VCP and VCX coil configurations have the transmitter dipole moment aligned vertically, transversely and longitudinally respectively with regards to the flight direction. The AEM data consists of the in-phase (*R*, real response) and quadrature (*Q*, imaginary response, relative to the primary field from the transmitter) signals detected by the receiver coils. The phase (φ) of the response is given by $\varphi = \arctan(R/Q)$.

The first AEM bathymetry survey in Australia took place in 1998 over Sydney Harbour (New South Wales, Australia) using a DIGHEM^V system (Figure 2a), originally developed by Fraser (1978) for resistivity mapping of metallic mineral deposits in the 1970s using earlier DIGHEM versions. The DIGHEM^V system is an analogue instrument[6] consisting of 5 coil pairs (3 HCP and 2 VCX, Table 1). The lowest frequency (*f*) was tuned to 328 Hz to

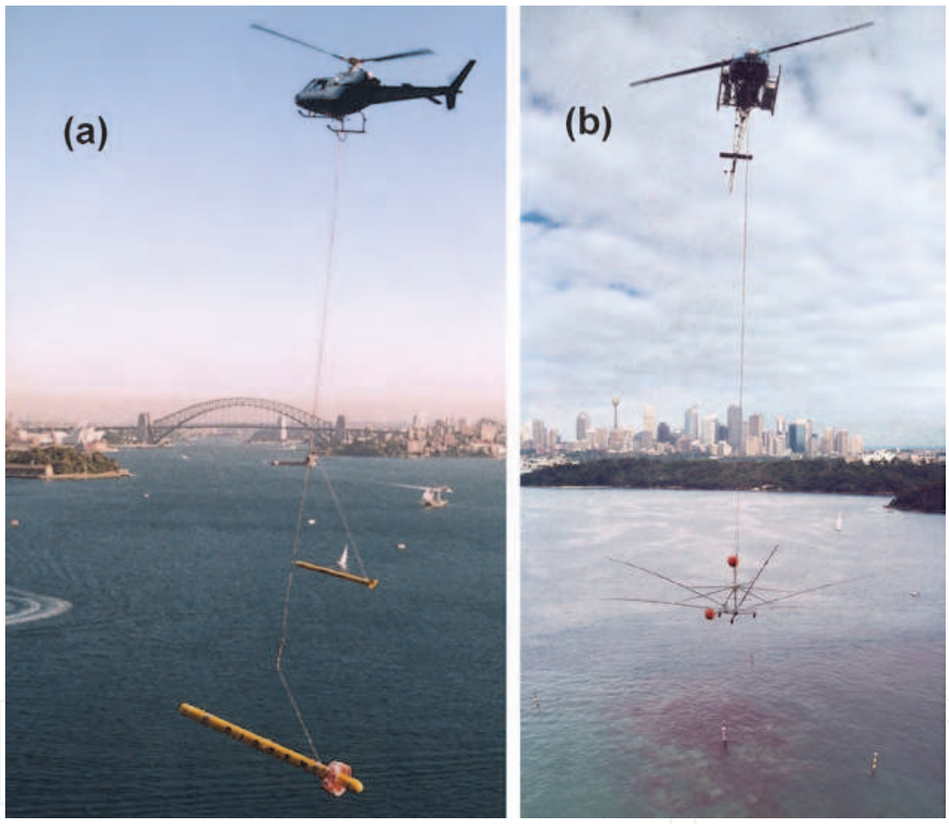

Fig. 2. (a): the frequency-domain helicopter DIGHEM^V AEM system (~ 8 m length) during survey over Sydney Harbour (Vrbancich, et al., 2000a,b). The smaller bird between the helicopter and the DIGHEM bird is a magnetometer bird; (b): The HoistEM time-domain helicopter AEM bird, located over the Sow and Pigs reef during a survey of Sydney Harbour (Vrbancich & Fullagar, 2004, 2007b). The transmitter loop (~ 22 m diameter) is attached to the extremities of the poles and the multi-turn receiver loop is located on the same plane, at the centre of the system.

[6] The current system is the digital RESOLVE system, used in Australia for example to study salinisation, e.g. Hatch et al., (2010).

maximise the depth of penetration through seawater, i.e., to increase the skin depth (δ) where δ (m) = $500/(\sigma.f)^{1/2}$ = $250/(f)^{1/2}$ for a typical seawater conductivity (σ) of 4 S/m. Following this survey, Shoalwater Bay (Queensland, Australia; Vrbancich, 2004) and Sydney Harbour have been surveyed using an analogue DIGHEM_Res(istivity) instrument with 5 HCP coil pairs operating within the range of 387 Hz to 103 kHz (Table 1).

	f1 (Hz)	f2 (Hz)	f3 (Hz)	f4 (Hz)	f5 (Hz)
DIGHEM(V)	328 HCP	889 VCX	5658 VCX	7337 HCP	55300 HCP
Skin Depth: δ (2δ)	13.8 (27.6)	8.4 (16.8)	3.3 (6.6)	2.9 (5.8)	1.1 (2.2)
Resistivity Bird	387 HCP	1537 HCP	6259 HCP	25800 HCP	102700 HCP
Skin Depth: δ (2δ)	12.7 (25.4)	6.4 (12.8)	3.2 (6.4)	1.6 (3.2)	0.8 (1.6)

Table 1. Frequencies and associated skin depths (m) for the DIGHEM^{V} and DIGHEM-Resistivity AEM birds. Skin depth δ (m) assumes a typical seawater conductivity of 4 S/m. Depth of investigation is equivalent to approximately 2δ (m).

One advantage of FEM helicopter AEM systems (compared to fixed-wing TEM systems) is that the transmitter and receiver coils are contained in a rigid structure so that the coils are held in a fixed position relative to each other. However pendulum motion of the towed bird generates a geometric and inductive effect in the measured EM response and contributes to altimeter error (Davis et al., 2006). If the bird swing period can be determined from survey data, a filter can be designed to remove bird swing effects, to first order, caused by pendulum motion (Davis et al., 2009). Predictions of bird swing from GPS receivers mounted on the bird and the helicopter can be used to predict the bird maneuver (Davis et al., 2009; Kratzer & Vrbancich, 2007). Calibration errors in FEM helicopter data can be identified by transforming the data to several different response-parameter domains and used to minimise the effect of altimeter and bird maneuver errors (Ley-Cooper et al., 2006). Importantly, this procedure can be applied to historic data, i.e., previous/dated FEM helicopter AEM data can be re-analysed with this procedure.

3.2 Fixed-wing time-domain AEM

A TEM system does not use a continuous sinusoidal current to power the transmitter loop (as in FEM systems). Instead, typically, the transmitter current is increased to a maximum value (during the "on-time"), and then reduced to "zero" current and measurements are made during the "off-time" when the transmitter is not powered[7]. Two examples of TEM waveforms are shown schematically in Figure 3. The secondary magnetic fields related to the decay of the induced currents in the ground are detected whilst there is no primary field. The process is repeated using the same current pulse but with the opposite polarity and the same off-time interval (Figure 3), and this response is subtracted from the first response to

[7] On-time measurements are also possible with some TEM systems but are not discussed here. The TEM fixed-wing and helicopter TEM systems used for AEM bathymetry studies in Australia use data recorded only during the off-time.

improve the signal to noise ratio. The period of the waveform (consisting of the the two on-time periods (Δt_1) of opposite polarity and their corresponding off-time periods, Δt_2) represents the base frequency($1/\Delta t_3$), Figure 3; 25 Hz is used in Australia and 30 Hz is used in America to minimise 50 Hz and 60 Hz power line transmission interference respectively. The results of the subtraction between the measurements made during the first and second halves of the waveform are stacked (averaged) over many cycles to reduce noise.

The shape of the recorded waveform (transient decay, Figure 3c) during the off-time is equivalent to the response at a number of frequencies (ranging high to low) for a harmonically varying source. Thus different sections of the decay curve contain different proportions of high and low frequency components. Morrison et al. (1969) computed the vertical component of the transient field from an airborne horizontal loop above a layered ground and observed that at early times (shortly after the transmitter current has dropped to zero), the response is due to both high and low frequency components whilst at later times approaching the end of the off-time interval, only the low frequency response

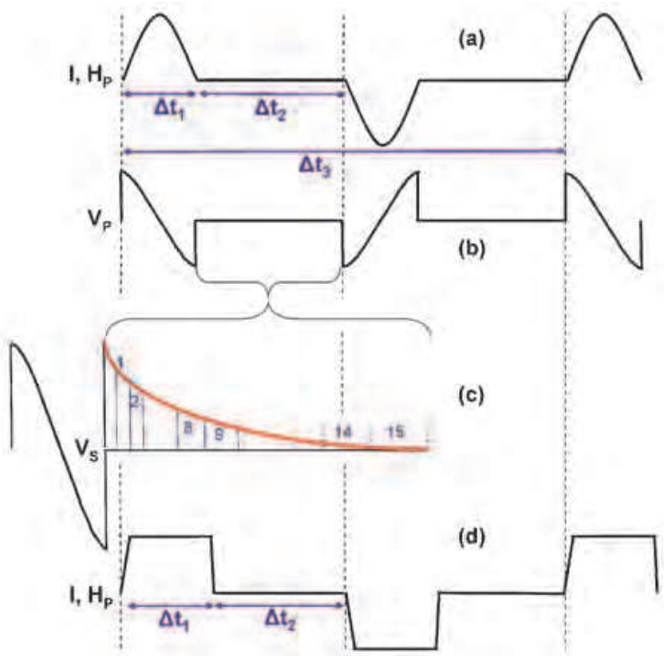

Fig. 3. Current and voltage waveforms. (a): Half-sine bipolar wave pulse – transmitter current (I) and primary magnetic field (H_P) waveform (e.g. GEOTEM, QUESTEM). On-time (Δt_1) typically 4 ms, off-time (Δt_2), typically 16 ms. For a base frequency of 25 Hz (Δt_3 = 40 ms), $\Delta t_1 + \Delta t_2$ = 20 ms (half period). (b): Voltage (V_P) from primary field at the receiver loop, or at high altitude where there is no response from the ground, i.e., no voltage (V_S) from secondary magnetic fields. (c): Response from ground (V_S) during off-time: transient decay curve (EM response) shown in red, sampled typically 120 to 250 times and binned into typically 15 to 30 windows (approximately logarithmically spaced) with narrow windows at early times to capture rapid decay and wider windows at late times to capture slower decays. (d) Quasi-trapezoidal current waveform (e.g. HoistEM, RepTEM, SeaTEM), 25 Hz base frequency, on-time (Δt_1) typically 5 ms, off-time (Δt_2), typically 15 ms, typically 21 to 28 windows. Not to scale.

remains. Morrison et al (1969) also noted that given that the skin depth is inversely proportional to the square root of the frequency, then the early part of the transient decay is governed by rapid decay of high frequency energy which has only penetrated down to relatively shallow depths whilst at later times, the response is dominated by lower frequency energy which has penetrated to greater depths. Resistive media are associated with a rapid decay, conductive media are associated with a longer decay. For bathymetric applications, early time (and higher frequency) AEM data are required for shallow seawater depths and late time (and low frequency) AEM data are required for deeper seawater. In principle, the lower the base frequency for TEM systems and the lower the frequency for FEM systems, then the greater the depth of investigation in seawater.

3.2.1 Variable transmitter-receiver geometry

Fixed-wing TEM systems have the transmitter coil spanning the wingtips and front and rear extremities of the aircraft, as shown schematically in Figure 1, with the receiver coil contained in a "bird" that is released from the rear of the aircraft. The transmitter and receiver operate at different heights above ground level. The aircraft survey altitude is typically about 120 m and the bird has an assumed fixed horizontal offset within the range of 90 to 120 m and an assumed fixed vertical offset within the range of 40 to 60 m, relative to the centre of the transmitter. Unlike FEM helicopter systems, the relative geometry between the receiver and transmitter is variable leading to interpretation errors arising from unrecorded variations of bird attitude, offset and altitude, thereby limiting the potential of the AEM bathymetry method. Vrbancich & Smith (2005) estimated bird position errors of several metres at survey altitude using GEOTEM data, based on the prediction of the vector components of the primary field measured by the receiver at high altitude, i.e. assuming a free-space approximation (Smith, 2001a) and at survey altitude over conductive seawater by estimating the distortion of the primary field caused by an in-phase contribution to the primary field from the seawater response (Smith, 2001b). These approximate methods for determining bird position only have an accuracy of a few metres and may therefore be limited. Another method involving the determination of bird position and receiver coil attitude as parameters obtained in a least-squares sense during layered-earth inversion of multi−component datasets (Sattel et al., 2004) has been applied to GEOTEM data to significantly improve the bathymetric accuracy of an AEM bathymetry survey in Torres Strait, located between Australia and Papua New Guinea (Wolfgram & Vrbancich, 2007).

3.3 Helicopter time domain AEM

Helicopter TEM systems are similar to the fixed-wing systems except that both the transmitter and receiver loops are located on a framework suspended as a sling load beneath the helicopter, as shown in Figure 2b. The waveforms are similar to those of fixed-wing TEM systems, i.e., an on-time period followed by an off-time period (Figure 3). Sattel (2009) has reviewed current helicopter TEM systems. The VTEM (Geotech Ltd.; Witherly, 2004) and HeliGEOTEM/HELITEM (Smith et al., 2009) systems for example are typically used for mineral exploration and the SkyTEM system (Sorensen & Auken, 2004) was developed for hydrogeophysical and environmental applications. The HoistEM (Boyd, 2004) and RepTEM systems have been used for several AEM bathymetry surveys in Australian

coastal waters (e.g. Sections 4.2-4.4), together with the SeaTEM system (e.g. Section 4.5) which was developed alongside the RepTEM system[8] specifically for bathymetric applications. An example of the SeaTEM waveform is shown schematically in Figure 3d. The HoistEM, RepTEM and SeaTEM systems are central loop systems with the receiver loop and transmitter loops co-axially aligned and lying within the same plane (i.e., nominally no vertical separation between the loops).

3.4 AEM footprint

The AEM footprint is a measure of the lateral resolution of an AEM system and was originally studied for frequency-domain AEM in the context of sea ice measurements by Liu & Becker (1990). The AEM footprint, in the inductive limit, was defined as the square area centred beneath the transmitter that contained the induced currents responsible for 90% of the observed secondary magnetic field detected at the receiver (Liu & Becker, 1990). The inductive limit refers to the case of a perfect conductor and/or infinite transmitter frequency, and as such, the induced currents are entirely in-phase with the primary field (i.e. no quadrature component) and the Liu-Becker footprint therefore corresponds to the minimum in-phase footprint of a frequency-domain AEM system. In the case of finite transmitter frequency and earth conductivity, the currents induced in the earth will have a larger spatial extent than that at the inductive limit (Beamish, 2003) and will contain both in-phase and quadrature components. Reid & Vrbancich (2004) have compared the inductive-limit footprints of various AEM configurations including time-domain systems in order to analyse the suitability of AEM systems for Antarctic sea-ice thickness measurements. Reid et al. (2006) extended the Liu-Becker footprint calculations (Liu & Becker, 1990; Reid & Vrbancich, 2004) to the case of finite frequency and earth conductivity for HCP and VCX configurations over an infinite horizontal thin sheet and for a homogeneous half-space. This study found that AEM footprint sizes may be several times the Liu-Becker inductive-limit value, with the quadrature footprint approximately half to two-thirds that of the in-phase footprint.

The Liu-Becker footprint is determined by both the transmitter-receiver geometry and the altitude (h). For a dipole-dipole frequency-domain AEM configuration with a transmitter-receiver separation of 6.3 m, the Liu-Becker footprint is 3.73h and 1.35h for HCP and VCX coil geometries. For a central loop system (e.g. HoistEM), the footprint is 3.68h, see Table 2 for a comparison of footprint sizes between several AEM systems. Beamish (2003) also computed the AEM footprint, using a different definition based only on the current system induced in the earth by the transmitter neglecting the contributions the secondary magnetic fields induced by currents in the ground make at the receiver. Beamish determined footprint sizes of between 0.99h and 1.43h for a horizontal magnetic dipole source (transmitter), and between 1.3h and 2.1h for a vertical magnetic dipole source, depending on the transmitter frequency and half-space conductivity. Section 4.4 presents an example of how the EM footprint affects the lateral and vertical resolution using 1D inversion.

[8] The HoistEM system was developed by the Normandy Group and the RepTEM and SeaTEM systems were developed by Geosolutions Pty.Ltd. The RepTEM system recently replaced the HoistEM system.

System	Tx height	Rx height	Tx-Rx separation	Geometry	Footprint/Tx-height
DIGHEM	30 m	30 m	8.0 m	HCP	3.72
				VCX	1.34
				VCP	1.44
SkyTEM	30 m	30 m	0.0	Tx(z)-Rx(z)	3.68
GEOTEM	120 m	70 m	130.0 m	Tx(z)-Rx(z)	4.51
				Tx(z)-Rx(x)	2.97

Table 2. Liu-Becker inductive-limit footprint sizes (footprint to transmitter height ratios) for several common AEM systems. Tx: transmitter, Rx: receiver. For TEM systems, the geometry is specified by the directions of the Tx and Rx dipole axes: Tx(z)-Rx(z) denotes a vertical-axis Tx and vertical-axis Rx, Tx(z)-Rx(x) denotes a vertical axis Tx and a horizontal-axis (inline) Rx. For the central loop helicopter TEM configuration (e.g. SkyTEM, HoisTEM), the Tx loop was a finite horizontal loop (10 m x 10 m) and the Rx was a vertical axis point dipole. Adapted from Table 1, Reid & Vrbancich (2004).

4. AEM bathymetry studies in Australian coastal waters

In 1998, the Australian Hydrographic Service (formerly known as the Royal Australian Navy Hydrographic Service) and the Defence Science & Technology Organisation (DSTO) began investigating the use of AEM as a rapidly-deployable bathymetric mapping technique in Australian waters,[9] complementing the use of lidar. Commercial systems were initially used from 1998 to 2005 for field trials to appraise the accuracy of the AEM bathymetry method based on (i) time-domain fixed-wing AEM using the GEOTEM and QUESTEM systems (Vrbancich et al., 2005a,b; Wolfgram & Vrbancich, 2007), (ii) time-domain helicopter AEM using the HoistEM system (Vrbancich & Fullagar, 2004, 2007b) and (iii) frequency-domain helicopter AEM using the DIGHEM^V system (Vrbancich et al., 2000a,b) and DIGHEM_Resistivity system (Vrbancich, 2004). Between 2006 and 2010, field trials were conducted with a prototype SeaTEM system (Vrbancich, 2009), a floating system equivalent to the commercial RepTEM system (Vrbancich et al., 2010) and the SeaTEM system (Vrbancich, 2011; Vrbancich, 2010). The SeaTEM system is essentially a slightly smaller version of RepTEM, developed for DSTO by Geosolutions Pty Ltd. as a research instrument. The results of the floating AEM system were significant, providing an upper limit to the accuracy expected from AEM systems similar to the RepTEM central loop system.

4.1 Sydney Harbour – helicopter frequency-domain AEM (DIGHEM)

A DIGHEM^V survey undertaken in 1998 (Vrbancich et al., 2000a) was flown over the width of the entrance to Sydney Harbour including the Sow and Pigs reef located in the centre of the channel. The nominal bird height was 30 m. Two interpretation methods were used to

[9] The scope for testing the potential use of AEM for bathymetric mapping is significant, especially within waters affected by turbidity and in the surf zone. Within the Australian Charting Area, the area of waters less than 70 m in depth that are considered to be *well* surveyed by any method, is estimated to be about 599,000 square kilometres. The areas of waters less than 50 m and between 50 to 70 m in depth that are considered to be *poorly* surveyed are estimated to be about 531,000 and 867,000 square kilometres respectively. It is also estimated that approximately 30% of the waters within the 70 m depth contour are affected by turbidity. (Australian Hydrographic Service, personal communication, 2010.)

estimate the water depths: direct layered-earth (1D) inversion and the conductivity-depth transform (CDT). The former method uses program *AEMIE* (Fullagar Geophysics Pty Ltd) based on a modified version of a 1D inversion program for horizontal loop EM (Fullagar & Oldenburg, 1984) and the latter method is a rapid approximation method not relying on inversion, to achieve fast processing and interpretation (Macnae et al., 1991; Wolfgram & Karlik, 1995; Fullagar, 1989) using program *EMFlow* (Macnae et al., 1998). The concept of the conductivity-depth transform is crudely described as follows. For each time in the transient decay (Figure 3c), the conductivity of a homogeneous half-space is computed such that the predicted magnetic field amplitude matches the observed field at that given time. Thus providing the field amplitude at a series of times gives the apparent conductivity[10] (σ_a) at each time *t*. This process associates a set of apparent conductivities with the decay times ($\sigma_a \Leftrightarrow t$ **)**, and the depths (*d*) of the "smoke ring" diffusing through the homogeneous ground as a function of time is associated with a set of times ($d \Leftrightarrow t$), thus the apparent conductivity is associated via time with depth (conductivity-depth transform, $\sigma_a \Leftrightarrow d$ **).**

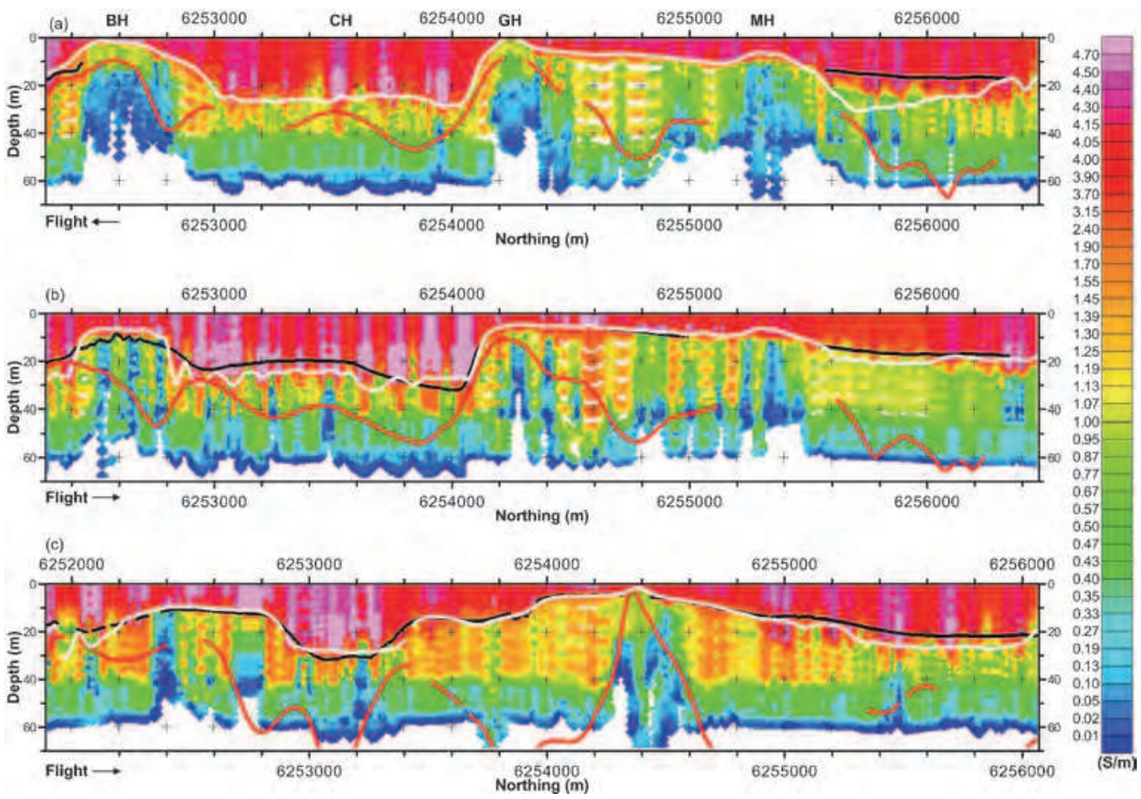

Fig. 4. *AEMI* (layered-earth inversion) conductivity sections (S/m) with profiles of depth to bedrock from seismic surveys (red), echo sounding water depths (black) and Geoterrex-DIGHEM proprietary inversion software (white). (a): this line skirts the coastline and lies closest to the headlands, marked BH, CH, GH and MH; (b) and (c) progress further away from the coastline; line spacing is nominally 50 m. Source: Vrbancich et.al., 2000b.

[10] The apparent conductivity is the conductivity of a homogeneous half-space which will give rise to the same EM response as that that would be measured over a real earth.

The results of a layered earth inversion for three adjacent flight lines that flank four sandstone headlands are shown in Figure 4. For this inversion, four layers were assumed in the starting model overlying a resistive basement. If conductivities greater than about 2.5 S/m are attributed to seawater, the inverted conductivity-depth sections are in good agreement with known water depths, even in the deeper regions of ~ 30 m. The equivalent conductivity-depth sections obtained from the conductivity-depth transform using program *EMFlow* is shown in Figure 5. (Both Figures 4 and 5 use the same colour scale bar.) The interpreted seawater layer has a higher average conductivity than the layered earth inversion, typically about 6 S/m (measured conductivity was 4.5 – 4.6 S/m). Generally however, there is very good agreement with measured water depth soundings, especially down to about 20 m. This comparison shows that the conductivity-depth transform method can provide useful bathymetric data quickly, but the interpreted water depths for this dataset are not quite as accurate as those obtained from layered-earth inversion.

The features in Figures 4, 5 that are less conductive than seawater and more conductive than the resistive bottom layer (i.e., coloured orange-yellow-green) are indicative of unconsolidated marine sediments. The very shallow marine sediments indicating bedrock at or near the seafloor is clearly identified where the survey line is closest to the headlands

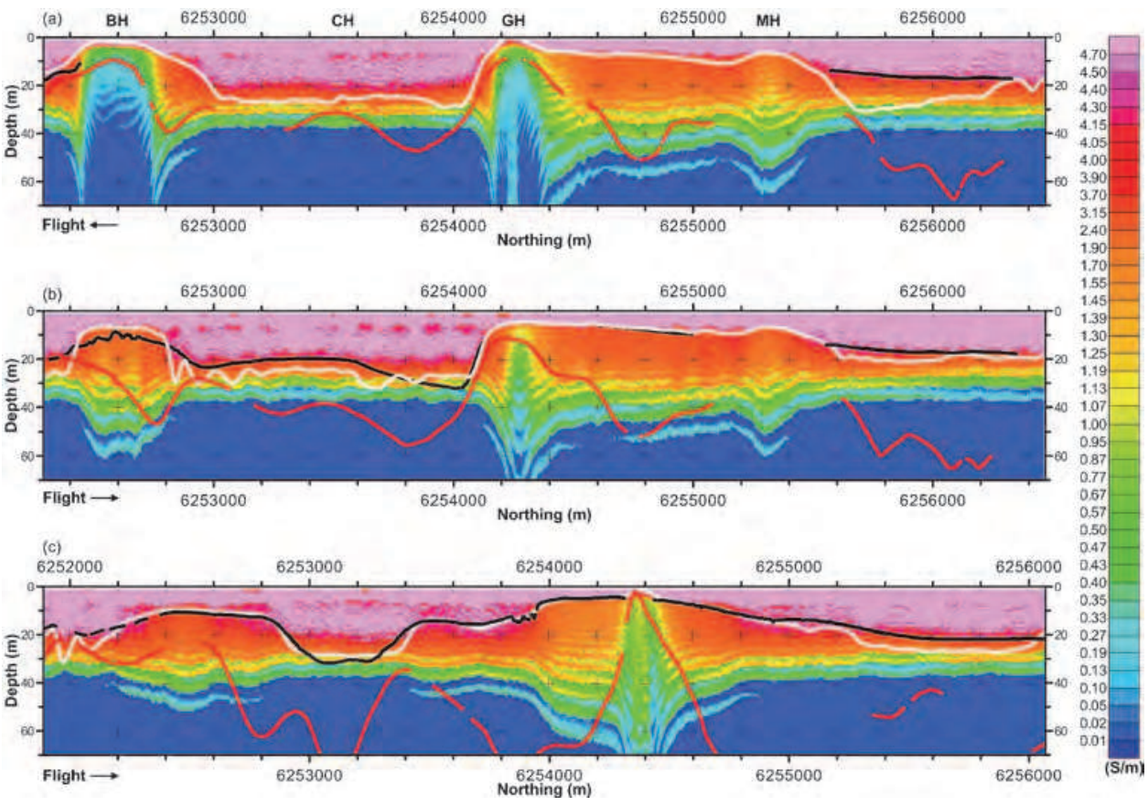

Fig. 5. *EMFlow* (conductivity-depth transform) conductivity sections (S/m) with profiles of depth to bedrock from seismic surveys (red), echo sounding water depths (black) and Geoterrex-DIGHEM proprietary inversion software (white). (a): this line skirts the coastline and lies closest to the headlands, marked BH, CH, GH and MH; (b) and (c) progress further away from the coastline; line spacing is nominally 50 m. Source: Vrbancich et.al., 2000b.

marked BH, GH and MH in Figures 4a and 5a. The seismic profiles (shown in red) were obtained from an earlier study (Emerson & Phipps, 1969). Another marine seismic study (Harris et al., 2001) confirms that the bedrock reaches the seafloor adjacent to the headland MH at a depth predicted by the AEM data as shown in Figures 4a, 5a, and that the seismic line in Figures 4b, 5b adjacent to the headland BH is incorrect and that the actual bedrock contour in this region is in agreement with that predicted by the AEM data (Figure 5b).

4.2 Sydney Harbour – helicopter time-domain AEM (HoistEM)

Sydney Harbour was resurveyed again in 2002 using the HoistEM time-domain helicopter AEM system (Figure 2b). The AEM data were improperly calibrated (Vrbancich & Fullagar, 2004) and was corrected using a procedure that reconciles the measured data with available ground truth at selected points within the survey (Vrbancich & Fullagar, 2007b). An example of a conductivity section resulting from a line that was flown over the Sow and Pigs reef is shown in Figure 6. A two-layer-over-basement model was used for the inversion. The fitted upper layer conductivity agrees well with the measured seawater conductivity and the seawater-sediment interface accurately follows the known water depth profile (yellow), mostly to within 1 m or better. The maximum depth of investigation was found to be ~ 55 – 65 m, just offshore of the harbour entrance. The time-domain equivalent of the skin depth is the diffusion length (δ_{TD}) given by $\delta_{TD} = \sqrt{2t/\sigma\mu_0}$ where σ is the conductivity (S/m) and μ_0 is the magnetic permeability of free space. Assuming a seawater conductivity of 4 to 5 S/m, δ_{TD} corresponds to a depth of 76 to 68 m respectively at the late time (t) of 14.4 ms and this represents an estimate of the maximum depth of investigation for this AEM system. Vrbancich & Fullagar (2007a) also showed that this dataset, and hence the AEM technique, has the potential to identify the coarse features of the underlying bedrock topography, as partly revealed in Figure 6.

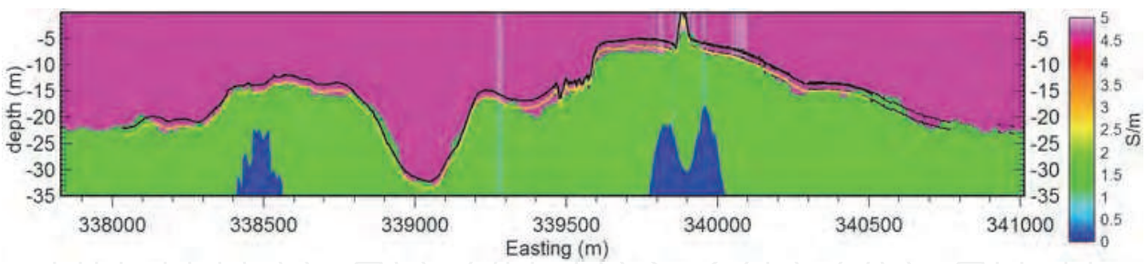

Fig. 6. Conductivity-depth sections from 1D inversion using corrected data to account for imperfect AEM instrument calibration. Accurate bathymetry profiles (obtained from combined multi-beam sonar and lidar data) are shown: (i) tide corrected (black) referred to a given datum; (ii) actual water depth at time of survey (yellow), which includes a tide height of 1.4 m. The Sow and Pigs reef is shown as a pinnacle at ~ 339900 m (E). The colour scale has units of S/m. Measured seawater conductivity is ~ 4.7 S/m. The green section represents sediment and the blue sections represent underlying resistive basement (bedrock). Source: Vrbancich & Fullagar, 2007b.

Figure 7 compares 3D images of the seafloor topography (defined by the water depth); the lower image is derived from inversion of corrected AEM data and was obtained by interpolating the water depth profiles defined by the seawater-sediment interface depth, as

shown Figure 6, to a gridded surface (i.e. by gridding the depth profiles). The upper image was obtained by gridding the known water depths. For the purpose of this comparison, individual known bathymetry grids from several high-spatial density sonar surveys and airborne laser depth soundings were combined into a single grid and sampled at the HoistEM measurement locations (fiducial point coordinates) to produce bathymetric data at the relatively low spatial density of the AEM data, e.g., the black and yellow curves in Figure 6. Gridding the series of yellow curves across all the survey lines yields the upper image in Figure 7.

4.3 Crookhaven Bight – helicopter time-domain AEM (SeaTEM)

Figure 8 shows a representative example of a profile (line L1185, red) of interpreted water depths obtained from layered-earth inversion of SeaTEM data, from a survey flown over Crookhaven Bight (~ 35.0° S, 150.8° E) in November 2009, adjacent to Jervis Bay and located approximately 150 km south of Sydney. The western section of the profile joins Currarong Beach and this section and the coastal area adjacent to the beach follows the seafloor gradient accurately (compare with black and grey profiles obtained from sonar data) to a water depth of about 25 to 30 m. The peaks at ~ 301400 and 302300 m (E) arise from reef structure, identifying a cross-section of the "zig-zag" nature of palaeochannels incised into the bedrock, as shown by the troughs located at 301800 and 301300 m (E) (Vrbancich et al., 2011).

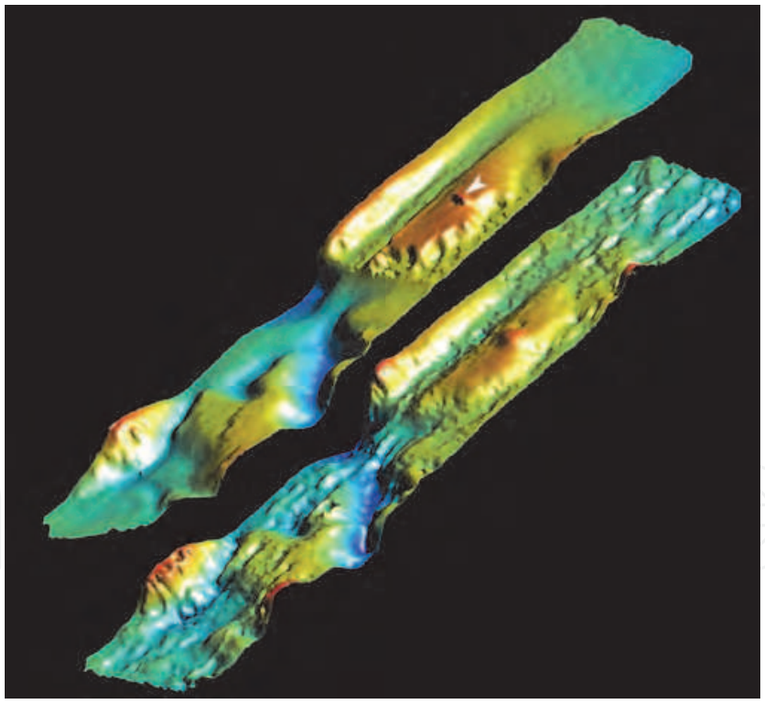

Fig. 7. Three-dimensional images of the seafloor topography based on pre-existing sonar-lidar data (top) and on inversion of corrected HoistEM data (bottom). Inverted seawater depths were not smoothed prior to gridding. The images are vertically aligned and are depicted with the same vertical exaggeration and colour scale. The surface is coloured according to water depth: red (0-4 m); orange (< 7m); yellow (<10 m); pale green (< 16 m); aqua (< 23 m) and dark blue (< 32 m). The "white" arrowhead (top) marks the location of the Sow and Pigs reef. Source: Vrbancich & Fullagar, 2007b.

The AEM survey was flown using 30 lines with 100 m line spacing. A colour–shaded surface grid obtained by gridding all the 30 profiles is shown in Figure 9 and can be compared directly with an equivalent grid of the single-beam sonar data, shown in Figure 10. All of the significant features and most minor features are accurately identified in the AEM

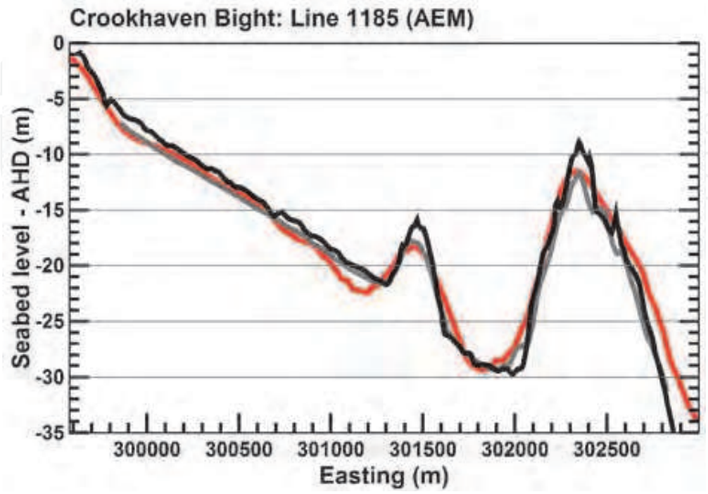

Fig. 8. Seabed level relative to Australian Height Datum (AHD) for survey line L1185; red: AEM bathymetry; black: Australian Hydrographic Service single-beam sonar data; grey: single-beam sonar data recorded during marine seismic survey (Vrbancich et al., 2011a). The location of this profile is shown in Figures 9 and 10.

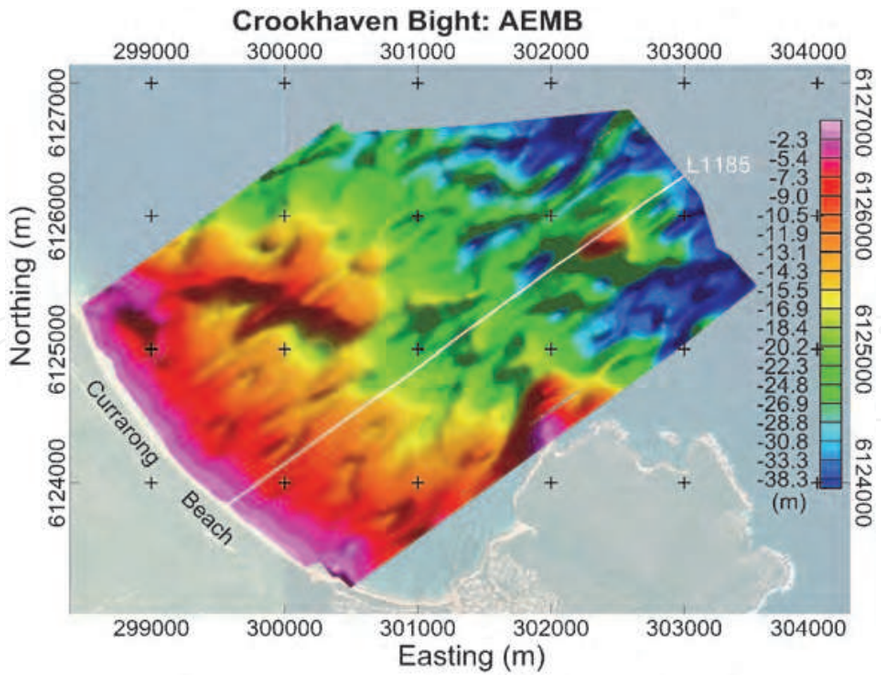

Fig. 9. Bathymetry of Crookhaven Bight survey area derived from AEM (SeaTEM) data. The bathymetry profile for line L1185 is shown in Figure 8 (red). The colour scale refers to the water level (m) relative to Australian Height Datum.

bathymetry map which took approximately 2 hours to survey and about 1 hour to process the data and run the inversions to produce a georeferenced map. The SeaTEM AEM system is experimental. In some regions, as shown in Figure 9, the interface depths display an oscillatory profile in some areas which degrades the accuracy of the derived water depths. Intensive tests conducted after this survey have shown that these anomalies may be caused by a high frequency noise source which cannot be removed by the usual data processing procedures. The source of this noise is currently being investigated.

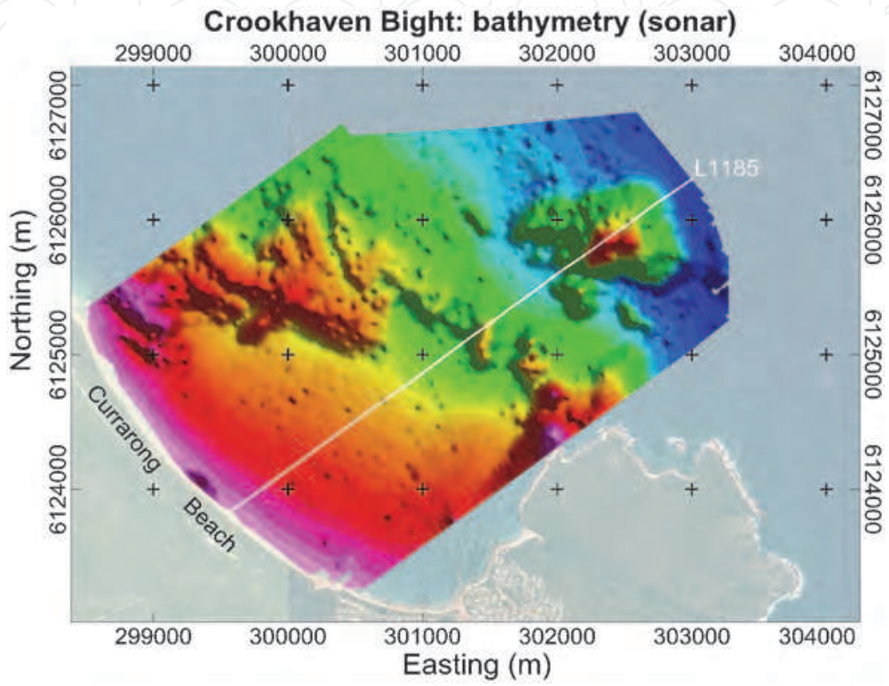

Fig. 10. Bathymetry of Crookhaven Bight survey area derived from sonar (Australian Hydrographic Service) data. The bathymetry profile for line L1185 is shown in Figure 8 (black). The colour scale is the same as shown in Figure 9.

4.4 Yatala Shoals – helicopter time-domain AEM (HoisTEM) – AEM footprint features

Yatala Shoals (~ 35.7° S, 138.2° E) is located in Backstairs Passage, South Australia, between the Fleurieu Peninsula and Kangaroo Island. This area is interesting because it contains a series of ridges, which fan out, increasing in separation and decreasing in height above the seafloor. This area was surveyed in 2003 using the HoistEM system, to examine the effect of the EM footprint on the lateral resolution, for resolving peak separation and height.

Figure 11 shows the results of layered-earth inversion for two profiles, separated by about 300 m. The main feature is a ridge rising approximately 18 m from the seafloor at ~ 244700 m (E) (Figure 11a) which gradually deepens and splits into two ridges (244390 and 244670 m (E), Figure 11b). A series of narrow ridges and troughs flank the eastern side of this main ridge. The impact of the AEM footprint is evident as a smoothing and underestimation of peak heights. Referring to the AEM bathymetry profiles (red), the narrow trough (~ 100 m gap) to the west of the main ridge in Figure 11a between 244400 and 244700 m (E) is unresolved, yet as this ridge splits into two ridges with a trough wider than 300 m (Figure

11b), the height and width of the western ridge (~ 244390 m (E)) is well resolved, and the secondary peak at 244670 m (E) is clearly resolved, yet its width is over determined and the height of the ridge is noticeably underestimated by about 3 m. The ridges that flank the eastern side of the main ridge are relatively narrow (~ 100 to 150 m) and are smaller than the central loop EM footprint, thus whilst the peaks are identified, their elevations above the seafloor are all underestimated by several metres. Another factor contributing to the apparent smoothing of the peak structure is the effect of assuming a 1D (layered-earth) model for inversion. 2D/3D modelling and inversion would be more appropriate in this case, however the routine use of *generalised* 3D modelling and inversion methods has not been realised, furthermore, the application of existing methods to an entire AEM survey dataset is impractical because of the required computer processing time. Cox et al. (2010) have recently introduced a robust 3D inversion scheme based on a moving AEM footprint that would enable the effects of the 1D approximation (i.e. assuming a layered-earth) to be fully investigated.

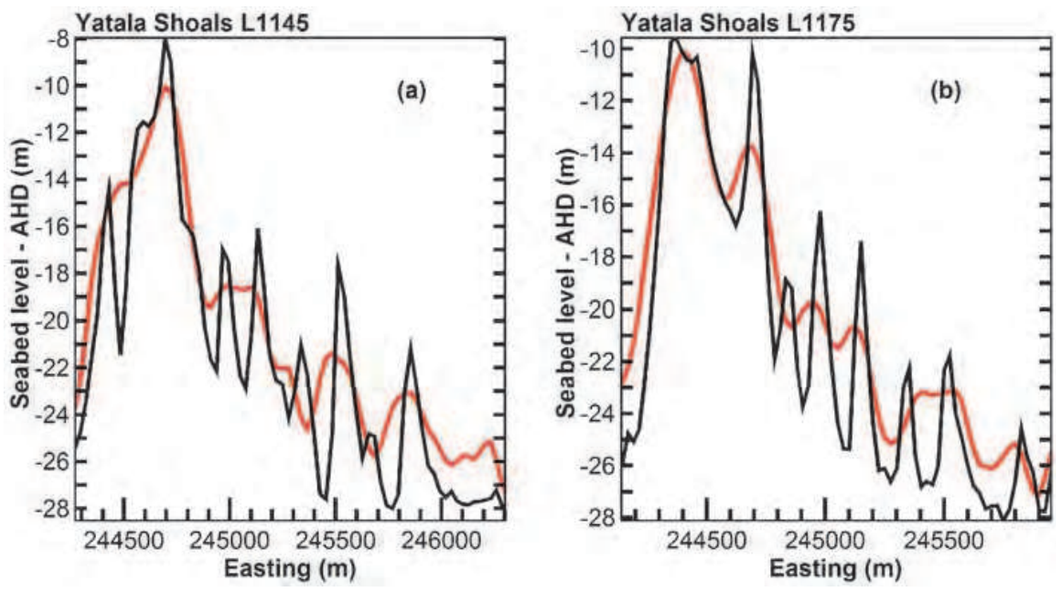

Fig. 11. Seabed levels, Yatala Shoals, relative to Australian Height Datum for HoistEM lines (a) L1145, (b) L1175, separated by approximately 300 m; red: AEM bathymetry; black: lidar.

4.5 Palm Beach (Broken Bay) – helicopter time-domain AEM (SeaTEM)

Figures 12a,b show a comparison of known bathymetry (sonar) and bathymetry derived from AEM data, obtained from a SeaTEM survey undertaken in 2009 over waters adjacent to Palm Beach, Broken Bay (~ 33.59^{o} S, 151.33^{o} E) located ~ 40 km north of Sydney Harbour. The depths were obtained using a two-layer-over-basement model using measured seawater conductivity, altimetry and a sediment conductivity of 1.25 S/m (consistent with sampled sediments in the region, Vrbancich et al., 2011b) as fixed parameters in the inversion. The AEM bathymetry map shows very good agreement with the known bathymetry, highlighting the gradual deepening of waters offshore Palm Beach, and the shoal region adjacent to Barrenjoey Head. A palaeochannel running approximately east-west was mapped, based on AEM data, about 60 m below marine sediments in this area, estimated to

cut across Palm Beach at ~ 628225 m (N). The extent and depth of the palaeochannel in this area was found to be in very good agreement with a depth-to-bedrock map derived from marine seismic data (Vrbancich et al., 2011b).

5. Discussion and conclusion

The use of AEM methods, traditionally applied to mineral exploration, can be applied to the measurement of water depths and seawater and seabed conductivity in shallow coastal waters that may be turbid and lie within the surf zone, thereby limiting the application of lidar techniques in these waters. The pioneering work in this area was carried out in Canada and the USA, with most of this work published in the 1980s and early 1990s[11]. This paper presents some of the findings of AEM bathymetry studies in Australian coastal waters carried out between 1998 and 2010 using helicopter frequency- and time-domain systems. The AEM footprint (and hence the lateral resolution) is significantly greater than the lidar footprint, and this limits the AEM method for bathymetric mapping where International Hydrographic Organisation (IHO) standards are required. However sub-metre vertical water depth resolution can be obtained using AEM methods in shallow waters (within a 10 to 20 m depth range). Presently, the AEM bathymetry method is a reconnaissance technique that can be rapidly deployed in remote areas via helicopter, for fast estimation of coastal water depths, including waters in the surf zone and turbid waters, to depths of about 30 to 40 m, and for identifying areas of exposed reef and for estimating the coarse features of the underlying bedrock topography.

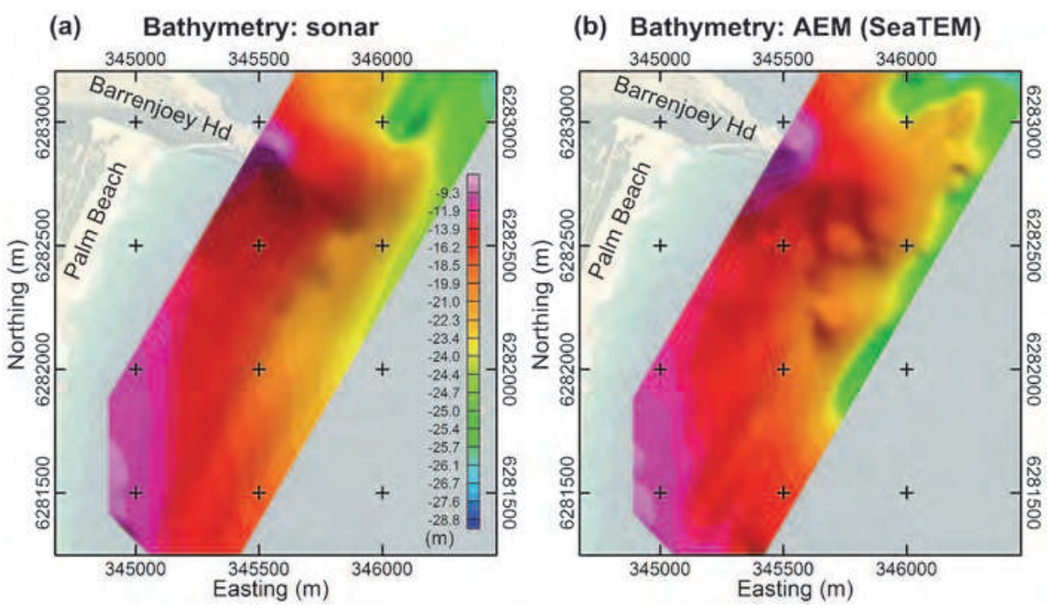

Fig. 12. Bathymetry maps of an area adjacent to Palm Beach, Broken Bay: (a), sonar; (b) AEM. Both maps use the same colour scale to show the seabed level relative to the Australian Height Datum.

[11] Many of the technical development issues, applications, recommended areas of research and strategies for further development, as discussed in a working group report in 1987 (Bergeron et al, 1987), are still relevant.

One of the most important issues is instrument calibration, affecting both environmental and exploration applications of AEM. Data obtained from (i) measurements of seawater depth and conductivity, (ii) sediment conductivity from bore hole samples and (iii) sediment depths estimated from marine seismic data, all acquired from a suitable trial site, can be combined to provide ground-truth data to establish a suitable geo-electrical model, for checking instrument calibration errors by comparing derived depths and conductivities with "known" depths and conductivities. Improved instrument calibration will lead to more robust estimates of seawater depth, seabed properties, sediment thickness and bedrock topography as well as improved depth accuracy and deeper depths of investigation.

Apart from improving AEM instrument calibration, reducing noise sources and including sensors to accurately track bird motion, future work will also involve software enhancements in program *AMITY* and associated software (Fullagar Geophysics Pty Ltd) to enable geologically-constrained 1D time-domain inversion, and 1D extremal inversion which enables models to be constructed with maximal and minimal characteristics (e.g. depth and conductivity bounds) which fit the observed data to within acceptable levels. Where warranted, future studies will also include the use of 3D EM modelling and inversion methods for interpretation of AEM data.

6. Acknowledgment

I thank Graham Boyd (Geosolutions Pty Ltd), Keith Mathews (Kayar Pty Ltd), Richard Smith (Technical Images Pty Ltd) and Peter Fullagar (Fullagar Geophysics) for their contributions to the AEM bathymetry (AEMB) studies in Australian waters. I thank the Australian Hydrographic Service for supporting AEMB and the Defence Imagery & Geospatial Organisation (DIGO) for release of aerial imagery under the NextView licence, as used in Figures 9, 10 & 12.

7. References

Archie, G.E. (1942). The Electrical Resistivity Log as an Aid in Determining Some Reservoir Characteristics. *Transactions American Institute for Mining, Metallurgical and Peroleum Engineers*, Vol. 42, pp. 54-62.

Beamish, D. (2003). Airborne EM Footprints. *Geophysical Prospecting*, Vol. 51, No. 1 (January 2003), pp. 59-60.

Becker, A. & Morrison, H.F. (1983). Analysis of Airborne Electromagnetic Systems for Mapping Thickness of Sea Ice. Prepared for NORDA, contract N62306-83-M-1755. Engineering Geoscience, University of California, Berkeley, November 1983.

Becker, A.; Morrison, H.F. & Zollinger, R. (1984). Airborne Electromagnetic Bathymetry. *SEG Expanded Abstracts*, Vol. 3, pp. 88-90.

Becker, A.; Morrison, H.F.; Zollinger, R. & Lazenby, P.G. (1986). Airborne Bathymetry and Sea-Bottom Profiling with the INPUT Airborne Electromagnetic System. In: *Airborne Resistivity Mapping, Geological Survey of Canada Paper 86-22*, G.J. Palacky (Ed.), pp. 107-109.

Bergeron, C.J., Jr.; Ioup, J.W. & Michel, G.A. (1989). Interpretation of Airborne Electromagnetic Data Using the Modified Image Method. *Geophysics*, Vol. 54, No. 8 (August 1989), pp. 1023-1030.

Bergeron, C.J. Jr.; Holladay, J.S.; Kovac, A.; Mozley, E.; Smith, B.D.; Watts, R.D. & Wright, D.L. (1987). Bathymetry and Related Uses Working Group Report. In: *Proceedings of the US Geological Survey Workshop on Development and Application of Modern Airborne Electromagnetic Surveys*, D. Fitterman (Ed.), October 7-9, 1987, pp. 204-205.

Boyd, G.W. (2004). HoistEM – A New Airborne Electriomagnetic System. *Conference Proceedings: PACRIM 2004*, ISBN: 9781920806187, Australian Institute of Mining and Metallurgy (September 2004), Adelaide, pp. 211-218.

Bryan, M.W.; Holladay, K.W.; Bergeron, C.J. Jr.; Ioup, J.W. & Ioup, G.E. (2003). MIM and Non-Linear Least-Squares Inversions of AEM Data in Barataria Basin, Louisiana. *Geophysics*, Vol. 68, No. 4 (July-August 2003), pp. 1126-1131.

Cox, L.H.; Wilson, G.A. & Zdanov, M.S. (2010). 3D Inversion of Airborne Electromagnetic Data Using a Moving Footprint. *Exploration Geophysics*, Vol. 41, No. 4 (December), pp 250-259.

Davis, A.C.; Macnae, J. & Robb, T. (2006). Pendulum Motion in Airborne HEM Systems. *Exploration Geophysics*, Vol. 37, No. 4 (December 2006), pp. 355-362.

Davis, A.; Macnae, J. & Hodges, G. (2009). Predictions of Bird Swing from GPS Coordinates. *Geophysics*, Vol. 74, No. 6 (November-December 2009), pp. F119-F126.

Dickinson, J.E.; Pool, D.R.; Groom, R.W. & Davis, L.J. (2010). Inference of Lithologic Distributions in an Alluvial Aquifer Using Airborne Transient Electromagnetic Surveys. *Geophysics*, Vol. 75, No. 4 (July-August 2010), pp. WA149-WA161.

Emerson,D.W. & Phipps, C.V.G. (1969). The Delineation of the Bedrock Configuration of Part of Port Jackson, New South Wales with a Boomer System. *Geophysical Prospecting*, Vol., 17, No. 3 (September 1969), pp. 219-230.

Fitterman, D.V. & Deszcz-Pan, M. (1998). Helicopter EM Mapping of Salt-Water Intrusion in Everglades National Park, Florida. *Exploration Geophysics*, Vol. 29, Nos 1 & 2, pp. 240-243.

Fountain, D. (1980). Airborne electromagnetic systems – 50 years of development. *Exploration Geophysics*, Vol. 29, Nos 1 & 2, pp. 1-11.

Fraser, D.C. (1978). Resistivity Mapping with an Airborne Multicoil Electromagnetic System. *Geophysics*, Vol. 43, No. 1 (February 1978), pp. 144-172.

Fullagar, P.K. & Oldenburg, D.W. (1984). Inversion of Horizontal Loop Electromagnetic Frequency Soundings. *Geophysics*, Vol. 49, No. 2 (February 1984), pp. 150-164.

Fullagar, P.K. (1989). Generation of Conductivity-Depth Pseudo-Sections from Coincident Loop and In-Loop TEM Data. *Exploration Geophysics*, Vol. 20, No., 1 & 2 (June, 1989), pp. 43-45.

Grant, F.S. & West, G.F. (1965). Interpretation Theory in Applied Geophysics. McGraw-Hill, New York.

Glover, P. (2009). What is the Cementation Exponent? A New Interpretation. *The leading Edge*, Vol. 28, No. 2 (January 2009), pp. 82-85.

Haas, C.; Gerland, S.; Eicken, H. & Miller, H. (1997). Comparison of Sea Ice Thickness Measurements Under Summer and Winter Conditions in the Arctic Using a Small Electromagnetic Induction Device. *Geophysics.*, Vol. 62, No. 3 (May-June 1997), pp. 749-757.

Haas, C.; Lobach, J.; Hendricks, S.; Rabenstein, L. & Pfaffling, A. (2009). Helicopter-borne Meaururements of Sea Ice Thickness Using a Small and Lightweight Digital EM System. *Journal of Applied Geophysics,* Vol. 67, No. 3 (March 2009), pp. 234-241.

Harris, G.A.; Vrbancich, J.; Keene, J. & Lean, J. (2001). Interpretation of Bedrock Topography Within the Port Jackson (Sydney Harbour) Region Using Marine Seismic Reflection. *15th Geophysical Conference of the Australian Society of Exploration Geophysicists,* Brisbane, Australia, 5-8 August 2001, *Extended Abstracts.*

Hatch, M.; Munday, T. & Heinson, G. (2010). A Comparative Study of In-river Geophysical Techniques to Define Variations in Riverbed Salt Load and Aid Managing River Salinization. *Geophysics*, Vol. 75, No. 4 (July-August 2010), pp. WA135-WA147.

Kirkegaard, C.; Sonnenborg, T.O.; Auken, E. & Jorgensen, F. (2011). Salinity Distribution in Heterogeneous Coastal Aquifers Mapped by Airborne Electromagnetics. *Vadoze Zone Journal*, Vol. 10, No. 1 (February 2011), pp. 125-135.

Kovacs, A. & Holladay, J.S. (1990). Sea-Ice Thickness Measurement Using a Small Airborne Sounding System. *Geophysics*, Vol. 55, No. 10 (October 1990), pp. 1327-1337.

Kovacs, A. & Valleau, C. (1987). Airborne Electromagnetic Measurement of Sea Ice Thickness and Sub-Ice Bathymetry. In: *Proceedings of the U.S. Geological Survey Workshop on Developments and Applications of Modern Airborne Electromagnetic Surveys*, D.V. Fitterman, (Ed.), 165-169, October 7-9, 1987.

Kovacs, A.; Holladay, J.S & Bergeron, C.J. Jr. (1995). The Footprint/Altitude Ratio for Helicopter Electromagnetic Sounding of Sea-Ice Thickness: Comparison of Theoretical and Field Estimates. *Geophysics*, Vol. 60, No. 2 (March-April 1995), pp. 374-380.

Kratzer, T. & Vrbancich, J. (2007). Real-Time Kinematic Tracking of Towed AEM Birds. *Exploration Geophysics*, Vol. 38, No. 2 (June 2010), pp. 132-143.

Ley-Cooper, Y.; Macnae, J.; Robb, T. & Vrbancich, J. (2006). Identification of Calibration Errors in Helicopter Electromagnetic (HEM) Data Through Transform to the Altitude-Corrected Phase-Amplitude Domain. *Geophysics*, Vol. 71, No. 2 (March-April 2006), pp. G27-G34.

Liu, G. & Becker, A. (1990). Two-Dimensional Mapping of Sea Ice Keels with Airborne Electromagnetics. *Geophysics*, Vol. 55, No. 2 (February, 1990), pp. 239-248.

Liu,G.; Kovacs, A. & Becker, A. (1991). Inversion of Airborne Electromagnetic SurveyData for Sea Ice Keel Shape. *Geophysics*, Vol. 56, No. 12 (December 1991), pp. 1986-1991.

Macnae, J.; Smith, R.; Polzer, B.D.; Lamontagne, Y. & Klinkert, P.S. (1991). Conductivity-Depth Imaging of Airborne Electromagnetic Step-Response Data. *Geophysics*, Vol. 56, No. 1 (January 1991), pp. 102-114.

Macnae, J.; King, A.; Stolz, N.; Osmakoff, A. & Blaha, A. (1998). Fast AEM Data Processing and Inversion. *Exploration Geophysics*, Vol. 29, No. 1 & 2 (June 1998), pp. 163-169.

Morrison, H.F.; Phillips, R.J. & O'Brien, D.P. (1969). Quantitative Interpretation of Transient Electromagnetic Fields Over a Layered Half Space. *Geophysical Prospecting*, Vol. 17, No. 1, (March 1969), pp. 82-101.

Morrison, H.F. & Becker, A. (1982). Analysis of Airborne Electromagnetic Systems for Mapping Depth of Seawater. Engineering Geoscience, University of California, Berkeley, California, Final report, ONR contract N00014-82-M-0073.

Mozley, E.C.; Kooney, T.N.; Byman, D.A & Fraley, D.E. (1991a). Kings Bay Airborne Electromagnetic Survey. Naval Oceanographic and Atmospheric Research

Laboratory, Marine Geosciences Division, Stennis Space Center, Report ID 019:352:91.

Mozley, E.C.; Kooney, T.N.; Byman, D.A & Fraley, D.E. (1991b). Airborne Electromagnetic Hydrographic Survey Technology. *SEG Expanded Abstracts*, Vol. 10, 468-471.

Nabighian, M.N. (1979). Quasi-static Transient Response of a Conducting Half-Space – an Approximate Representation. *Geophysics*, Vol. 44, No. 10 (October 1979), pp. 1700-1705.

Palacky, G.J. & West, G.F. (1991). Airborne Electromagnetic Methods. In *Electromagnetic Methods in Applied Geophysics – Volume 2 Applications Part B*, M.N. Nabighian, (Ed.), 811-879, Society of Exploration Geophysicists, ISBN 1-56080-22-4, Tulsa, Oklahoma.

Pelletier, R.E. & Holladay, K.W. (1994). Mapping Sediment and Water Properties in a Shallow Coastal Environment with Airborne Electromagnetic Profile Data: Case Study – the Cape Lookout, NC Area. *Marine Technology Society Journal*, Vol. 28, No. 2 (Summer 1994), pp. 57-67.

Pfaffling, A. & Reid, J.E. (2009). Sea Ice as an Evaluation Target for HEM Modelling and Inversion. *Journal of Applied Geophysics*, Vol. 67, No. 3 (March 2009), pp. 242-249.

Reid, J.E. & Macnae, J.C. (1998). Comments on the Electromagnetic "Smoke Ring" Concept. *Geophysics*, Vol. 63, No. 6, (November-December 1998), pp. 1908-1913.

Reid, J.E.; Vrbancich, J. & Worby, A.P. (2003a). A Comparison of Shipborne and Airborne Electromagnetic Methods for Antarctic Sea Ice Thickness Measurements. *Exploration Geophysics*, Vol. 34, Nos 1 & 2 (June 2003), pp. 46-50.

Reid, J.E.; Worby, A.P.; Vrbancich, J. & Munro, I.S. (2003b). Shipborne Electromagnetic Measurements of Antarctic Sea-Ice Thickness. *Geophysics*, Vol. 68, No. 5 (September-October 2003), pp. 1537-1546.

Reid, J.E. & Vrbancich, J. (2004). A Comparison of the Inductive-Limit Footprints of Airborne Electromagnetic Configurations. *Geophysics*, Vol. 69, No. 5 (September-October 2004), pp. 1229-1239.

Reid, J.E.; Pfaffling, A. & Vrbancich, J. (2006). Airborne Electromagnetic Footprints in 1D Earths. *Geophysics*, Vol. 71, No. 2 (March-April 2006), pp. G63-G72.

Sattel, D.; Lane, R.; Pears, G. & Vrbancich, J. (2004). Novel Ways to Process and Model GEOTEM data. *17th Geophysical Conference of the Australian Society of Exploration Geophysicists,* Sydney, Australia, 15-19 August 2004, *Extended Abstracts.*

Sattel, D. (2009). An Overview of Helicopter Time-Domain EM Systems. *20th Geophysical Conference of the Australian Society of Exploration Geophysicists,* Adelaide, Australia, 22-25 February 2009, *Extended Abstracts.*

Smith, R. (2001a). Tracking the Transmitting-Receiving Offset in Fixed-Wing Transient EM Systems: Methodology and Applications. *Exploration Geophysics*, Vol 32, No. 1 (March 2001), pp. 14-19.

Smith, R. (2001b). On Removing the Primary Field from Fixed-Wing Time-Domain Airborne Electromagnetic Data: Some Consequences for Quantitative Modelling, Estimating Bird Position and Detecting Perfect Conductors. *Geophysical Prospecting*, Vol. 49, No. 4 (July 2001), pp. 405-416.

Smith, R.S.; Hodges, R. & Lemieux, J. (2009). Case Histories Illustrating the Characteristics of the HeliGEOTEM System. *Exploration Geophysics*, Vol 40, No. 3 (September 2009), pp. 246-256.

Soininen, H.; Jokinen, T.; Oksama, M. & Suppala I. (1998). Sea Ice Thickness Mapping by Airborne and Ground EM Methods. *Exploration Geophysics*, Vol 29, Nos 1 & 2 (August 1998), pp. 244-248.

Son, K.H. (1985). Interpretation of Electromagnetic Dipole-Dipole Frequency Sounding Data Over a Vertically Stratified Earth. PhD thesis, North Carolina State University, Raleigh, 149 pp.

Sorensen, K.I. & Auken, E. (2004). SkyTEM – A New High-Resolution Helicopter Transient Electromagnetic System. *Exploration Geophysics*, Vol. 35, No. 3 (September 2004), pp. 194-202.

Spies, B.; Fitterman, D.; Holladay, S. & Liu, G. (Editors) (1998). Proceedings of the International Conference on Airborne Electromagnetics (AEM 98). *Exploration Geophysics* 1998, Vol. 29, Nos 1 and 2 (August 1998), pp. 1-262.

Vrbancich, J.; Hallett, M. & Hodges, G. (2000a). Airborne Electromagnetic Bathymetry of Sydney Harbour. *Exploration Geophysics*, Vol. 31, No. 1&2 (June 2000), pp. 179-186.

Vrbancich, J.; Fullagar, P.K. & Macnae, J. (2000b). Bathymetry and Seafloor Mapping via One Dimensional Inversion and Conductivity Depth Imaging of AEM. *Exploration Geophysics*, Vol. 31, No. 4 (December 2000), pp. 603-6.

Vrbancich, J. (2004). Airborne Electromagnetic Bathymetry Methods for Mapping Shallow Water Sea Depths. *International Hydrographic Review*, Vol. 5, No. 3 (November 2004), pp. 59-84.

Vrbancich, J. & Smith, R. (2005). Limitations of Two Approximate Methods for Determining the AEM Bird Position in a Conductive Environment. *Exploration Geophysics*, Vol. 36, No. 4 (December 2005), pp. 365-373.

Vrbancich, J.; Sattel, D.; Annetts, D.; Macnae, J. & Lane, R. (2005a). A Case Study of AEM Bathymetry in Geographe Bay and Over Cape Naturaliste, Western Australia, Part 1: 25 Hz QUESTEM. *Exploration Geophysics*, Vol. 36, No. 3 (September 2005), pp. 301-309.

Vrbancich, J.; Macnae, J.; Sattel, D. & Wolfgram, P. (2005b). A Case Study of AEM Bathymetry in Geographe Bay and Over Cape Naturaliste, Western Australia, Part 2: 25 and 12.5 Hz GEOTEM. *Exploration Geophysics*, Vol. 36, No. 4 (December 2005), pp. 381-392.

Vrbancich, J. & Fullagar, P.K. (2004). Towards Seawater Depth Determination Using the Helicopter HoistEM System. *Exploration Geophysics*, Vol. 35, No. 4 (December 2004), pp. 292-296.

Vrbancich, J. & Fullagar, P.K. (2007a). Towards Remote Sensing of Sediment Thickness and Depth to Bedrock in Shallow Seawater Using Airborne TEM. *Exploration Geophysics*, Vol. 38, No. 1 (March 2007), pp. 77-88.

Vrbancich, J. & Fullagar, P.K. (2007b). Improved Seawater Depth Determination Using Corrected Helicopter Time Domain Electromagnetic Data. *Geophysical Prospecting*, Vol. 55, No. 3 (May 2007), pp. 407-420.

Vrbancich, J. (2009). An Investigation of Seawater and Sediment Depth Using a Prototype Airborne Electromagnetic Instrumentation System – A Case Study in Broken Bay, Australia. *Geophysical Prospecting*, Vol. 57, No. 4 (July 2007), pp. 633-651.

Vrbancich, J.; Whiteley, R.J. & Emerson, D.W. (2011a). Marine Seismic Profiling and Shallow Marine Sand Resistivity Investigations in Jervis Bay, NSW, Australia. *Exploration Geophysics*, Vol. 42, No. 2 (June 2011), pp. 127-138.

Vrbancich, J.; Whiteley, R.J.; Caffi, P. & Emerson, D.W. (2011b). Marine Seismic Profiling and Shallow Marine Sand Resistivity Investigations in Broken Bay, NSW, Australia. *Exploration Geophysics*, Vol. 42, No. 4 (December), 227-238, DOI 10.1071/EG11031.

Vrbancich, J.; Fullagar, P. & Smith, R. (2010). Testing the Limits of AEM Bathymetry with a Floating TEM System. *Geophysics*, Vol. 75, No. 4 (July-August 2010), pp. WA163-WA177.

Vrbancich, J. (2010). Preliminary Investigations Using a Helicopter Time-Domain System for Bathymetric Measurements and Depth-to-Bedrock Estimation in Shallow Coastal Waters – A Case Sudy in Broken Bay, Australia, *Proceedings OCEANS 2010 IEEE*, ISBN 9781424452217, Sydney, Australia, May 24-27, 2010, 9pp.

Vrbancich, J. (2011). AEM Applied to Bathymetric Investigations in Port Lincoln, South Australia – Comparison with an Equivalent Floating TEM System. *Exploration Geophysics*, Vol. 42, No. 3 (September, 2011), pp. 167-175.

Wait, J.R. (1982). *Geo-Electromagnetism*. Academic Press, ISBN 0-12-730880-6, New York.

Ward, S.H. & Hohman, G.W. (1987). Electromagnetic Theory for Geophysical Applications. In *Electromagnetic Methods in Applied Geophysics – Volume 1 Theory*, M.N. Nabighian, (Ed.), 131-311, Society of Exploration Geophysicists, ISBN 0-931830-51-6, Tulsa, Oklahoma.

Weaver, J.T. (1994). *Mathematical Methods for Geo-Electromagnetic Induction*. Research Studies Press Ltd., ISBN 0 86380 165 X, Taunton, Somerset, England.

West, G.F. & Macnae, J.C. (1991). Physics of the Electromagnetic Induction Exploration Method. In *Electromagnetic Methods in Applied Geophysics – Volume 2 Applications Part A*, M.N. Nabighian, (Ed.), 5-45, Society of Exploration Geophysicists, ISBN 1-56080-22-4, Tulsa, Oklahoma.

Witherly, K. (2004). The Geotech VTEM Time Domain Helicopter EM System. *SEG Expanded Abstracts,* Vol. 23, Section MIN 3.5 (October 2004), 1221-1224.

Wolfgram, P. & Karlik, G. (1995). Conductivity-Depth Transform of GEOTEM Data. *Exploration Geophysics*, Vol. 26, No. 2 & 3 (September 1995), pp. 179-185.

Wolfgram, P. & Vrbancich, J. (2007). Layered Earth Inversions of AEM Bathymetry Data Incorporating Aircraft Attitude and Bird Offset – A Case Study of Torres Strait. *Exploration Geophysics*, Vol. 38, No. 2 (June 2007), pp. 144-149.

Won, I.J. & Smits, K. (1985). Airborne Electromagnetic Bathymetry: Naval Ocean and Research Development Activity, NSTL, MS, NORDA Report 94.

Won, I.J. & Smits, K. (1986a). Characterization of Shallow Ocean Sediments Using the Airborne Electromagnetic Method. *IEEE Journal of Oceanic Engineering*, Vol. OE-11, No. 1 (January 1986), pp. 113-122.

Won, I.J.,& Smits, K. (1986b). Application of the Airborne Electromagnetic Method for Bathymetric Charting in Shallow Oceans. In: *Airborne Resistivity Mapping, Geological Survey of Canada Paper 86-22*, G.J. Palacky (Ed.), pp. 99-106.

Won, I.J. & Smits, K. (1987a). Airborne Electromagnetic Bathymetry. In: *Proceedings of the US Geological Survey Workshop on Development and Application of Modern Airborne Electromagnetic Surveys*, D. Fitterman (Ed.), October 7-9, 1987, pp. 155-164.

Won, I.J. & Smits, K. (1987b). Airborne Electromagnetic Measurements of Electrical Conductivity of Seawater and Bottom Sediments Over Shallow Ocean. *Marine Geotechnology*, Vol. 7, No. 1, (March 1987), pp. 1-14.

Zollinger, R.D. (1985). Airborne Electromagnetic Bathymetry. MSc thesis, University of California, Berkeley, California, 45 pp.

Zollinger, R.; Morrison, H.F.; Lazenby, P.G. & Becker, A. (1987). Airborne Electromagnetic Bathymetry. *Geophysics*, Vol. 52, No. 8 (August 1987), pp. 1127-1137.

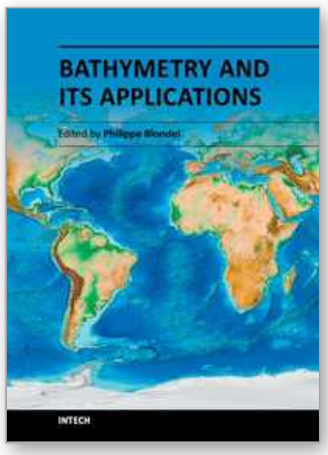

Bathymetry and Its Applications

Edited by Dr. Philippe Blondel

ISBN 978-953-307-959-2

Hard cover, 148 pages

Publisher InTech

Published online 25, January, 2012

Published in print edition January, 2012

Bathymetry is the only way to explore, measure and manage the large portion of the Earth covered with water. This book ,presents some of the latest developments in bathymetry, using acoustic, electromagnetic and radar sensors, and in its applications, from gas seeps, pockmarks and cold-water coral reefs on the seabed to large water reservoirs and palynology. The book consists of contributions from internationally-known scientists from India, Australia, Malaysia, Norway, Mexico, USA, Germany, and Brazil, and shows applications around the world and in a wide variety of settings.

How to reference

In order to correctly reference this scholarly work, feel free to copy and paste the following:

Julian Vrbancich (2012). Airborne Electromagnetic Bathymetry, Bathymetry and Its Applications, Dr. Philippe Blondel (Ed.), ISBN: 978-953-307-959-2, InTech, Available from: http://www.intechopen.com/books/bathymetry-and-its-applications/airborne-electromagnetic-bathymetry

INTECH
open science | open minds

InTech Europe
University Campus STeP Ri
Slavka Krautzeka 83/A
51000 Rijeka, Croatia
Phone: +385 (51) 770 447
Fax: +385 (51) 686 166
www.intechopen.com

InTech China
Unit 405, Office Block, Hotel Equatorial Shanghai
No.65, Yan An Road (West), Shanghai, 200040, China
中国上海市延安西路65号上海国际贵都大饭店办公楼405单元
Phone: +86-21-62489820
Fax: +86-21-62489821

IntechOpen